Signal Amplification Hot Paper

How to cite: *Angew. Chem. Int. Ed.* **2021**, *60*, 19974–19981
International Edition: doi.org/10.1002/anie.202107660
German Edition: doi.org/10.1002/ange.202107660

Mechanically Triggered Hybridization Chain Reaction

Yuxin Duan, Roxanne Glazier, Alisina Bazrafshan, Yuesong Hu, Sk Aysha Rashid, Brian G. Petrich, Yonggang Ke, and Khalid Salaita**

Abstract: *Cells transmit piconewton forces to receptors to mediate processes such as migration and immune recognition. A major challenge in quantifying such forces is the sparsity of cell mechanical events. Accordingly, molecular tension is typically quantified with high resolution fluorescence microscopy, which hinders widespread adoption and application. Here, we report a mechanically triggered hybridization chain reaction (mechano-HCR) that allows chemical amplification of mechanical events. The amplification is triggered when a cell receptor mechanically denatures a duplex revealing a cryptic initiator to activate the HCR reaction in situ. Importantly, mechano-HCR enables direct readout of pN forces using a plate reader. We leverage this capability and measured mechano-IC_{50} for aspirin, Y-27632, and eptifibatide. Given that cell mechanical phenotypes are of clinical importance, mechano-HCR may offer a convenient route for drug discovery, personalized medicine, and disease diagnosis.*

Introduction

The vast majority of cells dynamically generate mechanical forces through the polymerization/depolymerization of their cytoskeletal proteins. These forces are transmitted across the plasma membrane through transmembrane receptors, such as the integrin adhesion receptors, to mediate processes including migration, immune recognition, and differentiation.[1] Interestingly, adhesion receptors not only transmit forces, but also detect the magnitude of tension corresponding to the physical cues presented by other cells and the extracellular matrix.[2] Such forces are at the piconewton (pN) scale, and for reference, ≈7 pN applied over a distance of 1 nm is approximately 1 kcal mol^{-1}, which is diminishingly small and difficult to detect and investigate. Not only is measuring such forces of fundamental importance for understanding mechanisms of mechanotransduction, mechanics has also been shown as a diagnostic marker of cell state in a variety of pathologies.[3] For example, Sniadecki and colleagues found that the magnitude of traction forces generated by platelets from patients suffering from trauma was predictive of bleeding risk.[3a] Diminished platelet contractile forces are also reported by Lam and colleagues in patients with chronic bleeding symptoms.[3b] Thus, the development of molecular technologies to detect the pN forces transmitted by adhesion receptors can provide robust tools for clinical assays.

Molecular tension sensors provide a powerful method to detect the pN forces generated by cell receptors.[4] The first molecular tension sensors to detect cell receptor forces were described in 2011 and used an immobilized PEG polymer that was flanked with a fluorophore and quencher to optically detect receptor forces that drive stretching of the polymer.[4,5] Over the past decade, a suite of different classes of tension sensors comprised of nucleic acids,[6] proteins,[7] and polymers[5a] have been reported and applied to the study of a variety of mechanotransduction pathways, ranging from T cell[8] and B cell antigen recognition[9] to cell adhesion[6] and platelet activation (Table S1 and S2).[10]

Because receptor-mediated forces are highly transient (≈milliseconds to 10s of seconds), weak (≈pN), and fairly rare events (compared to ligand–receptor binding), these signals are difficult to quantify.[1c,8] One solution to this problem is to employ tension probes that irreversibly generate a fluorescence response to the pN input. The tension gauge tether (TGT) was originally developed by Ha and colleagues to control the forces transmitted by cells,[11] but later it was found that these probes could be modified with a fluorophore and quencher pair to report on the peak forces applied by cell surface receptors.[10a] The TGT is simply comprised of a DNA duplex, with one oligo anchored to the surface and the second oligo presenting a ligand specific to the receptor of interest. When the transmitted force exceeds a threshold value, called tension tolerance (T_{tol}), the duplex mechanically denatures, leading to de-quenching of the dye and generating a fluorescence signal proportional to the total number of accumulated mechanical events over time.[6,12] Nonetheless, the density of mechanical events is typically ≈100 events/μm^2.[8,13] Given the size of a typical mammalian cell of 100s of μm^2, at best each cell can generate a fluorescence signal corresponding to ≈10^3–10^4 fluorophores, which is difficult to quantify. Indeed, TGT signal quantification requires microscopes equipped with high NA objectives and single photon counting EMCCDs. Therefore, the instrumentation requirement hinders the widespread adoption of molecular tension probes for many applications including

[*] Y. Duan, A. Bazrafshan, Y. Hu, S. A. Rashid, Prof. K. Salaita
Department of Chemistry, Emory University
Atlanta, GA 30322 (USA)
E-mail: k.salaita@emory.edu
Dr. R. Glazier, Prof. Y. Ke, Prof. K. Salaita
Wallace H. Coulter Department of Biomedical Engineering
Georgia Institute of Technology and Emory University
Atlanta, GA 30322 (USA)
E-mail: yonggang.ke@emory.edu
Dr. B. G. Petrich
Department of Pediatrics, Emory University
Atlanta, GA 30322 (USA)
Supporting information and the ORCID identification number(s) for the author(s) of this article can be found under: https://doi.org/10.1002/anie.202107660.

high- and medium-throughput drug and cell screening, as well as integrating such assays into clinics.

Limited signal in bioanalytical chemistry is typically addressed by using enzymes such as horseradish peroxidase,[14] DNA polymerases, and more recently CRISPR nucleases (Cas12a and Cas13a) in assays such as ELISA and PCR.[15] These types of catalytic amplification assays have transformed modern biochemistry and are the cornerstone of the vast majority of clinical diagnostics. Developing amplification reactions that boost the signal generated by molecular tension probes is therefore highly desirable for mechanobiology and may open the door toward new areas, such as "mechanopharmacology" and "mechanodiagnostics" that can be potentially personalized using primary cells derived from patients.

Herein, we integrate the hybridization chain reaction (HCR) with molecular tension probes to generate a signal-amplification assay for readout of cell forces. HCR is an isothermal and enzyme-free reaction originally developed by Pierce and colleagues.[16] In HCR, two partially self-complementary hairpin oligonucleotides are designed with a large kinetic barrier to hybridization. The assembly of the two hairpins requires opening of one of the hairpins to propagate the formation of the DNA polymers, and this initiation is triggered by a toehold-mediated displacement reaction with a short DNA strand called the initiator (*I*, Figure 1 A). In mechano-HCR, the initiator is concealed and blocked by a complementary strand that is conjugated with a ligand to the receptor of interest. As is shown in Scheme 1 A, a DNA duplex is formed between a top strand conjugated to the ligand cyclo-Arg-Gly-Asp-Phe-Lys (cRGDfK) and a bottom strand anchored to the surface. When cells are seeded, membrane receptors such as integrins bind to the cRGDfK ligand on the duplex and apply forces. Forces that exceed the T_{tol} mechanically rupture the DNA duplexes, exposing the bottom strand (initiator) for triggering the HCR (Scheme 1 B). Subsequently, hairpin 1 (H1) and hairpin 2 (H2) are added to the well for HCR amplification (Supporting Information, Table S3 for DNA sequences).[17] Because the HCR polymerization reaction is fully compatible with cell culture media, the cells remain active during the amplification process. Importantly, the quantification of the mechano-HCR products can be achieved either by direct imaging with a fluorescence microscope or by using a plate reader. Because measuring cell traction forces can be performed in a multi-well plate, mechano-HCR allows one to screen many different cells that are subjected to different concentrations of drugs that can modulate cell mechanics. We demonstrate the potential significance of mechano-HCR by screening the

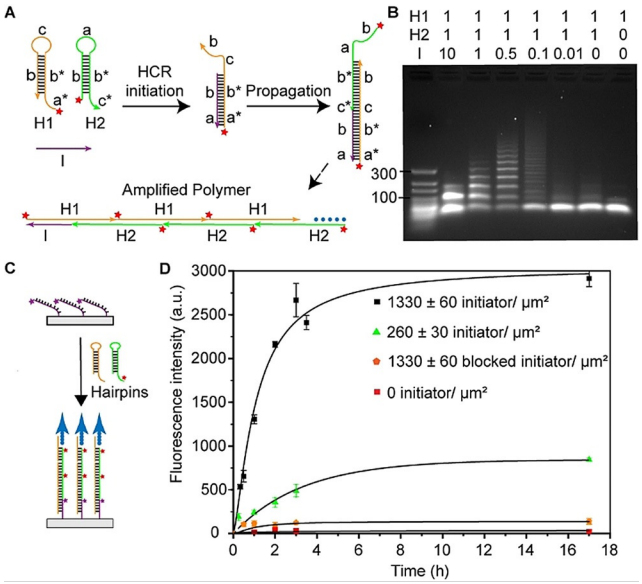

Figure 1. Validation of HCR using soluble and surface-anchored initiator. A) Schematic showing the different domains of H1, H2, and I that mediate the formation of HCR polymers. Small red star: Cy3B dye. B) Agarose gel image of HCR product with different hairpin-to-initiator ratio. Lanes from left to right: DNA ladder, 1:10 ratio, 1:1 ratio, 2:1 ratio, 10:1 ratio, 100:1 ratio, no initiator, and H1 only. 90 min reaction time, at RT, in 150 mM NaCl using [H1] = 1 μM. C) Schematic of surface-initiated HCR. D) Plot of time-dependent fluorescence intensity measured using fluorescence microscopy of surface polymerized H1 and H2-Cy3B. Error bar represents S.E.M. obtained from three independent experiments. The intensity of each surface at each time point was determined from 12 images randomly selected from different regions. The black line represents a pseudo-first order fit to $F.I.(t) = A(1-e^{-kt})$.

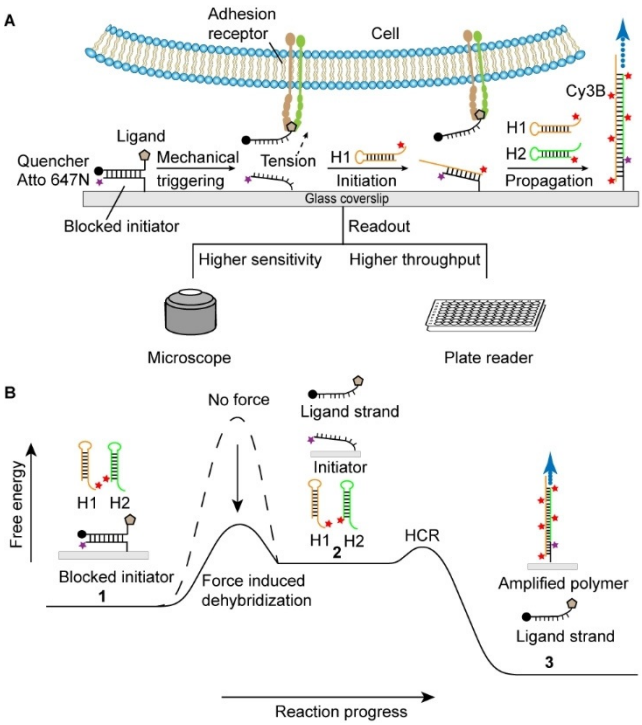

Scheme 1. The mechanically triggered hybridization chain reaction (mechano-HCR). A) Schematic showing the triggering mechanism to reveal a cryptic initiator that leads to local growth of a DNA polymer from two hairpin monomers (H1 and H2). In our work, the initiator is tagged with Atto647N while H1 and H2 are tagged with Cy3B. B) Idealized free energy landscape of mechano-HCR showing the transition from state **1** (blocked initiator, H1 and H2) to state **2** (exposed initiator, H1, and H2), and finally to the thermodynamic minimum state **3** with polymerized monomers. Theoretically, the barrier between **1** and **2** must be large and mechanical forces that denature the top strand are needed to lower this barrier (akin to a catalyst) and accelerate the rate of reaction by orders of magnitude.

activity of three drugs with anti-coagulation activity: aspirin, eptifibatide, ROCK-inhibitor. We find a high level of agreement between published IC_{50} (half-maximal inhibitory concentration) of these drugs and their mechano-IC_{50} measured by mechano-HCR. Therefore, this assay represents an important step toward rapid and automated screening of drugs that modulate cell mechanics.

Results and Discussion

To validate the activity of the HCR reaction, we used gel electrophoresis to detect polymerization products. We tuned the initiator concentration (from 0.01 to 10 μM) while maintaining a monomer hairpin concentration of 1 μM. The reactions were allowed to proceed in 150 mM NaCl for 1.5 h at room temperature (RT). Gel electrophoresis showed that decreasing initiator concentration produces longer HCR products, as anticipated, and the leakage rate of polymerization without initiator was minimal (Figure 1B). We also found that the HCR polymerization proceeds in cell culture medium with no significant change in reaction rate (Figure S1). Considering that immobilization of initiator imposes a steric constraint, we therefore studied the kinetics of HCR when the initiator was immobilized on a surface. In this assay, biotinylated single-stranded initiators were incubated on surfaces coated with streptavidin (Figure 1C). We tested different initiator incubation concentrations and found that the surface density of initiator reached maximum coverage when incubated at 100 nM for 1 h (Figure S2). We then used a quantitative fluorescence calibration employing supported lipid bilayer standards to determine the initiator surface density.[18] The result showed that the 100 nM incubation concentration led to an initiator density of 1330 ± 60 molecules/μm^2 while the 20 nM concentration produced a density of 260 ± 30 molecules/μm^2 (Figure S3). To trigger the HCR reaction, we added 62.5 nM of H1 and Cy3B-labeled H2 and imaged the surface at different time points (Figure S4). We next fit the rate of polymerization to a pseudo-first order reaction using these fluorescence–time plots and found that the surface HCR $t_{1/2} = 1.6 \pm 0.3$ h ($R^2 = 0.9942$, $t_{1/2}$ is the time needed to achieve half-maximum signal) when the initiator density equals 1330 molecule/μm^2 (Figure 1D). The $t_{1/2}$ indicated that a reaction time of 2 h for the live-cell mechano-HCR assay would be appropriate for sufficient signal amplification while limiting the total time of the assay.

We next applied the mechano-HCR assay to detect integrin-mediated forces applied by live cells. Integrin adhesion receptors are a family of heterodimeric receptors that span the plasma membrane and bridge the cellular cytoskeleton with the extracellular matrix (ECM) to mediate many processes including cell migration, adhesion, and immune recognition. Our past work, as well as the work of others including Ha and Wang, has showed that integrin receptors apply pN forces that are sufficient to mechanically denature DNA duplexes.[10a,19] Hence, measuring integrin forces within cell adhesions is an appropriate model to validate the mechano-HCR assay.

Firstly, we designed two types of DNA duplexes that have identical sequences and thermal melting temperatures, but different geometries and mechanical tolerance (Figure 2A).[11] In the unzipping geometry, mechanical forces denature the duplex, one base at a time, with a predicted $T_{tol} = 12$ pN, while in shearing geometry the duplex is more mechanically stable and has a predicted $T_{tol} = 60$ pN.[20] The cRGDfK ligand which has a high affinity to the $\alpha_v\beta_3$ integrin ($K_D = 1.3 \times 10^{-6}$ M[21]) was conjugated to the DNA duplex via

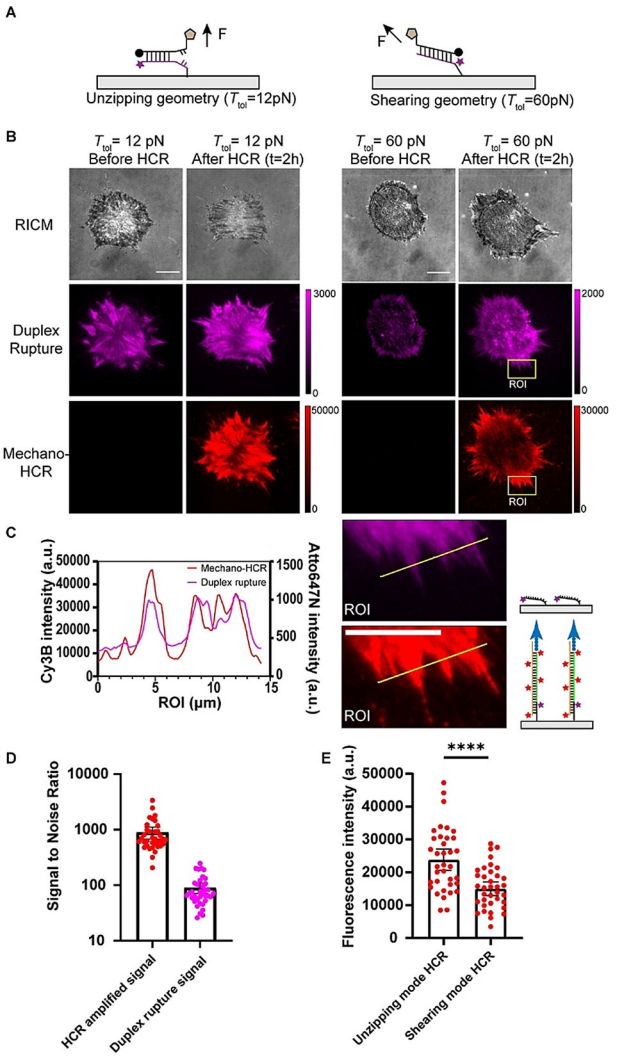

Figure 2. Mechano-HCR for live-cell mapping of cell traction forces. A) Schematic of DNA duplex with cryptic initiator used to study integrin-mediated forces. B) Representative RICM and fluorescence images of cells cultured on $T_{tol} = 12$ pN and $T_{tol} = 60$ pN surfaces before and after HCR amplification. Scale bar = 12 μm. The magenta color is emission from Atto647N tagging the initiator while the red channel shows the Cy3B emission from H1 and H2 following HCR. The intensity bar next to each fluorescence image shows the absolute signal intensity for each image. C) Plot of line scan and zoom in of the ROI from (B). Scale bar = 10 μm. D) Bar graph shows S/N of mechano-HCR and initiator rupture signal. Error bars represent S.E.M. from 36 cells in $n = 4$ independent experiments. E) Plot of fluorescence intensity of mechano-HCR using probes in the unzipping and shearing geometries. Error bars represent S.E.M. from 36 cells in $n = 3$ independent experiments (**** $p < 0.0001$, student t-test).

copper(I)-catalyzed azide–alkyne cycloaddition. HPLC, agarose gel electrophoresis, and MALDI-TOF characterization of the products confirm successful conjugation (Figure S5). cRGDfK-conjugated and fluorophore-quencher-tagged DNA duplexes were then immobilized onto the surface. Note that piranha etching of the glass slide is critical as slides activated using other protocols (base etching and plasma etching) showed high background and low reproducibility. NIH/3T3 fibroblast cells were then seeded on these surfaces for 1 h. As expected, we observed an increase in fluorescence signal for the 12 pN and 60 pN probes due to mechanical denaturation of the duplex (Figure 2B). We next added the H1 and H2 hairpin monomers to fuel the HCR and allowed the reaction to proceed for 2 h. After rinsing away the excess monomers, we observed strong HCR signals at the 2 h time point (Figure 2B). We found that the probes in the unzipping geometry were more significantly denatured compared to shearing mode probes (60 pN), in agreement with literature. Importantly, the 12 pN unzipping mode probes also generated a greater HCR signal, reflecting the greater density of exposed initiator (Figure 2E, Figure S6).

To demonstrate real-time tracking of the growth of mechano-HCR signals, we applied total internal reflection fluorescence microscopy (TIRF). As is shown in Figure S7, the mechano-HCR signal increased as a function of time and plateaued at $\approx$3–3.5 h. The real-time amplification of the HCR signal for one representative cell is provided in Supplementary Movie 1. Note that in our live-cell experiments, we did not notice significant steric hindrance of mechano-HCR (Figure S8).

Line scan analysis of representative regions of interest from different cells (Figure 2C) confirms that the mechano-HCR signal and probe rupture signals are highly colocalized, based on the measured Pearson's correlation coefficient of 0.80 ± 0.08 ($n = 40$ cells). However, the mechano-HCR signal is not perfectly colocalized with the initiator exposure signal in the fluorescence images. There are likely three reasons for the discrepancy. First, mechanical events that lead to unblocking of the initiator accumulate continuously over the 2 h duration and hence mechanical events that occur earlier in time lead to greater amplification. Second, HCR polymerization is inherently heterogeneous and generates polymers with significant polydispersity as recently discussed by Figg and colleagues.[22] Third, regions with limited number of duplex ruptures may only be detectable using mechano-HCR but not with exposed initiators.

To test whether single z-slice imaging can capture the majority of HCR signals, we next acquired z-stack images of mechano-HCR and DNA duplex rupture signal with a confocal microscope. As is shown in Figure S9 and Supplementary movie 2, the majority of HCR and duplex rupture signals are located next to the interface, indicating single Z-slice imaging is suitable for mechano-HCR quantification.

One important figure of merit when employing amplification strategies in analytical sensing is the signal-to-noise ratio (S/N) of the amplified signal. To quantify this value, we directly compared the S/N of the mechano-HCR and initiator unblocking signals. By using the standard deviation of the background (regions outside of the cell) as the "noise" and quantifying the fluorescence under the cell as the signal, we estimate that the mechano-HCR S/N $= 890 \pm 105$ ($n = 36$ images), which is much greater than the S/N for the probe denaturation signal $= 89 \pm 9$ ($n = 36$) (Figure 2D). Control DNA duplexes with no cRGDfK ligands incubated with cells and hairpins did not show significant initiator exposure or mechano-HCR signal (Figure S10). To verify the specificity of mechano-HCR to adhesion complexes, GFP–vinculin mouse embryonic fibroblasts were cultured on these surfaces and probed using our mechano-HCR assay. In these experiments we found a high degree of localization between focal adhesions (GFP) and the mechano-HCR signal based on the measured Pearson's correlation coefficient of 0.81 ± 0.05 ($n = 15$ cells from 3 independent experiments, Figure S11). These results further confirm that the mechano-HCR readout can be used to detect and amplify integrin-mediated tension in live cells and that this signal localizes to active focal adhesions in cells. Another potential merit of mechano-HCR is that mechano-HCR can be combined with super-resolution techniques including super-resolution radial fluctuations (SRRF) to improve the resolution of images (Figure S12).[23] We used SRRF because it offers high speed and live-cell compatibility and is fairly simple to implement without any hardware modification to a conventional wide-field microscope.

Given that integrin tension plays important roles in cell function, assays that can quantify the molecular traction forces of cells in a rapid fashion are desirable. One can envision applications for mechano-HCR in screening dose–response curves for drugs that modulate cell mechanics.[24] To achieve these goals, we first validated the mechano-HCR assay by plating an escalating density of NIH/3T3 cells in 96 well plates and measured the associated signal in each well. We expected the mechano-HCR signal to linearly increase as a function of cell density until the surface is fully covered with cells. In these experiments, we measured the exposed initiator density and compared this to the mechano-HCR signal using a fluorescence microscope. We chose the 12 pN duplex probe in the following experiments because the unzipping probe generates greater signals for both NIH/3T3 cells and mouse platelets, and hence facilitates readout in a plate reader (Figure S6). We found a highly linear relationship between the density of initiator sites (ruptured duplexes) and the final HCR signal (Figure S13). Because of the strength of the mechano-HCR signal, we next were able to measure the signal using a conventional plate reader. In agreement with the microscopy data, the bulk plate reader data showed a linear relationship between the number of plated cells and the fluorescence signal up to saturating cell densities (cell number $\approx$20000/32 mm^2, Figure 3A,B). Importantly, amplification was critical, as the probe rupture signal (Atto647N) was not detectable above the background using the plate reader, thus demonstrating that the relatively low S/N ratio of that readout is insufficient for automated plate reader analysis (Figure S14).

We next tested the potential of using mechano-HCR in screening the dose–response function for different small molecules that target cell mechanics. We first investigated the Rho kinase inhibitor, Y-27632, which targets the phosphor-

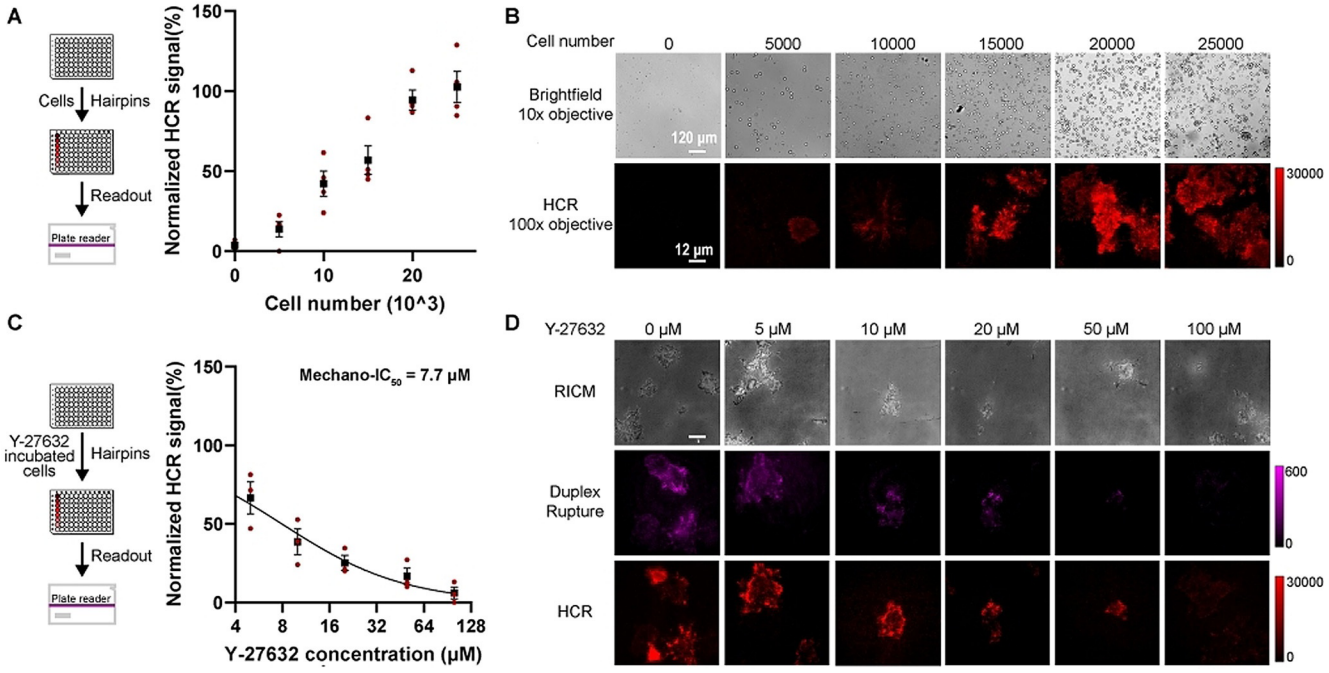

Figure 3. Mechano-HCR to detect cell forces using a plate reader. A) Schematic and plot showing plate reader mechano-HCR signal as a function of the number of cells seeded. A 96 well plate was used for these measurements. Error bar represents S.E.M. from 4 independent experiments, the individual experiments are shown as small red dots while the mean is indicated by black squares. The values were normalized to the signal obtained from the 25 000 cells/well samples. All measurements were background-subtracted using negative control wells lacking cells. There is a strong correlation between the number of cells plated and the mechano-HCR signal. Note that at cell numbers greater than 20 000, the signal plateaus. B) Representative bright field (10× objective) and mechano-HCR fluorescence (100× objective) from 96 well plates used to measure the signal as a function of cell number. C) Schematic and plot of plate-reader-measured mechano-HCR signal as a function of Y-27632 concentration. Drug was incubated for 30 min prior to seeding. Error bar represents S.E.M. from 3 independent experiments. Mechano-IC_{50} was calculated by fitting plot to a standard dose–response function: normalized signal = $100/(1+[\text{drug}]/IC_{50})$. The values were normalized to the signal obtained from the 20 000 cells/well samples without drug treatment. All measurements were background-subtracted using negative control wells lacking cells. D) Representative RICM and initiator rupture (magenta) and mechano-HCR (red) fluorescence images from wells used in dose–response measurement. Scale bar = 12 μm.

ylation of myosin light chain[25] and thus is known to dampen forces transmitted by focal adhesions. We pretreated NIH/3T3 cells with a range of Y-27632 concentrations (0–100 μM) for 30 min.[19a] The treated cells were then plated on 96 well plates presenting the 12 pN DNA duplex for 1 h, which was followed by mechano-HCR amplification and readout. We were satisfied to see that the mechano-HCR signal showed a dose-dependent reduction in intensity as a function of increasing ROCK inhibitor concentration (Figure 3C,D), indicating that plate-reader-based mechano-HCR readout reported cell traction forces modulated by MLC inhibition. By fitting the data to a standard dose–response inhibition function (signal = $100/(1+[\text{drug}]/IC_{50})$), we found that the mechano-IC_{50} = 7.7 μM (95 % CI = 5.8–10.2 μM), which is in agreement with the reported $IC_{50} \approx 5$ μM that was obtained with cell morphology and kinase assays.[26] We plotted the fluorescence intensity obtained from microscopy imaging in these experiments in Figure S15. A two-way ANOVA analysis was performed to compare the plate reader and the microscopy normalized mechano-HCR signal, which showed no significant difference between these two modes for measuring the dose–response curve.

Finally, to demonstrate mechano-HCR dose–response screening of drugs in primary cells, we investigated the mechanical signal of platelets under the influence of different antiplatelet drugs. Platelets are well suited for this type of screen because contractile forces are central in the function of platelets in resisting blood shear flow and in mechanically sealing off wound sites. Several platelet receptors such as glycoprotein Ib and integrin adhesion receptors have been identified as mechanosensors that mediate these functions.[27] Moreover, abnormal force generation in human platelets is related to clotting disorders which can be mediated by genetic mutations as shown by Lam and colleagues[3b] as well as trauma-induced coagulopathy as demonstrated recently by Sniadecki et al.[3a] Therefore, rapid detection of platelet tension may offer new tools for diagnostic screening. We tested three drugs that target platelet coagulation function: ROCK inhibitor Y-27632, which inhibits MLC phosphorylation (as described above), integrin $\alpha_{IIb}\beta_3$ antagonist eptifibatide, an FDA approved anti-clotting drug,[28] and aspirin, which inhibits the activity of cyclooxygenase (COX) and prevents formation of thromboxane A2 and thus functions as an anti-coagulation agent.[29] In these experiments, we incubated purified mouse platelets with each drug at room temperature for 30 min. Then we plated 2×10^6 mouse platelets in each well for 1 h and then performed the mechano-HCR assay. At the completion of the assay, and for each drug concentration tested, we measured the 12 pN duplex rupture signal (Atto647N) as well as the mechano-

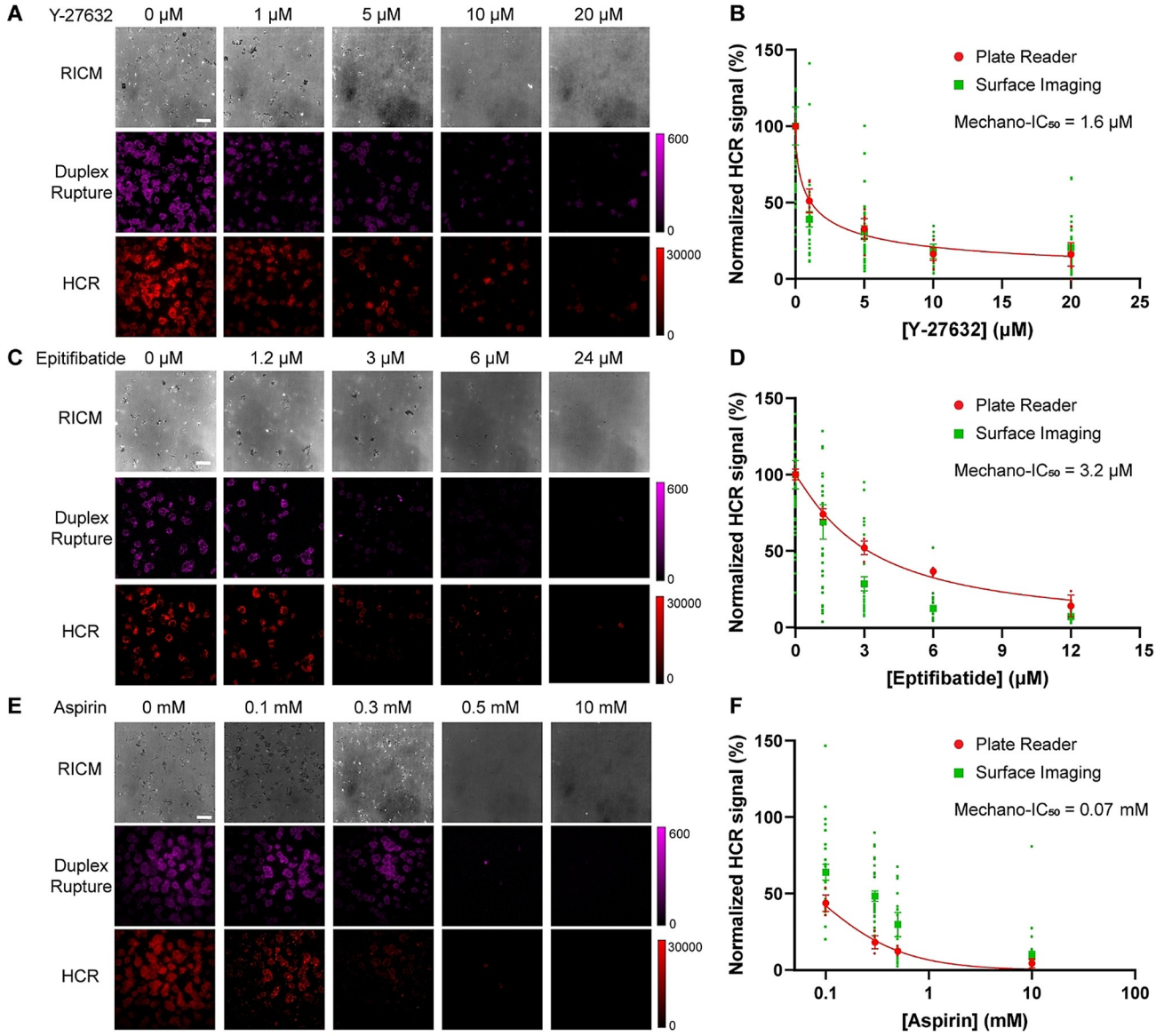

Figure 4. Using mechano-HCR to determine mechano-IC_{50} of platelet inhibitors. (A), (C), and (E) show representative RICM and initiator duplex rupture (magenta) and mechano-HCR (red) fluorescence images of mouse platelets that were treated with the ROCK inhibitor Y-27632, eptifibatide, and aspirin, respectively. Cells were treated with each drug for 30 min prior to mechano-HCR. Scale bar = 12 μm. 2×10^6 cells were seeded in each well. (B), (D), and (F) show plots of normalized mechano-HCR signal as a function of Y-27632, eptifibatide, and aspirin concentration, respectively. Error bar represents S.E.M. from $n=3$ independent animal samples for plate reader readout, and $n=30$ cells from three independent animal samples for imaging-based readout. The values were normalized to the signal obtained from the 2×10^6 cells/well samples without drug treatment. All measurements were background-subtracted using negative control wells lacking cells. Mechano-IC_{50} was calculated by fitting plate reader tension readout to normalized signal = 100/(1 + [drug]/IC_{50}). The red data points are the mechano-HCR signals measured using a plate reader while the green data points were obtained using a fluorescence microscope from individual platelets.

HCR signal (Cy3B) using both plate reader and high-resolution fluorescence microscopy. For all the compounds tested, we observed a dose-dependent decrease in the 12 pN duplex rupture in microscopy images (magenta color in Figure 4 A,C,E). Imaging of the same regions of interest in the mechano-HCR channel showed nearly identical signal patterns (red color in Figure 4 A,C,E) based on the measured Pearson's correlation coefficient of 0.76 ± 0.07 ($n=30$ cells from 3 independent experiments). The agreement between these two fluorescence channels confirmed that mechano-HCR robustly amplified the density of initiator that was mechanically exposed by platelets.

We next took these same 96 well plates and measured the signal in the Cy3B channel using a conventional plate reader and this intensity was plotted alongside the average intensities obtained from optical microscopy (Figure 4 B,D,F). The plots for each dose–response curve represent the signal averaged from $n=3$ animals. The unamplified 12 pN DNA duplex rupture signal in the Atto647N channel was not detectable. As expected, the plate reader signal reflected the microscopy data and showed a dose-dependent decrease in the intensity

for each well. A two-way ANOVA analysis comparing the plate reader and the microscopy mechano-HCR signal showed no significant difference between these two modes for measuring the dose–response curve. Furthermore, the difference in signal intensity between different doses tested was statistically significant regardless of the readout mode ($P < 0.0001$). By fitting the dose–response plots from the plate reader, we determined that the mechanical IC_{50} values for Y-27632, eptifibatide, and aspirin were 1.6 μM (95% CI = 0.98–2.5 μM), 3.2 μM (95% CI = 2.6–3.8 μM), and 0.07 mM (95% CI = 0.06–0.09 mM), respectively. These values were found to be similar to reported IC_{50} values in the literature (1 μM for Y-27632,[30] 5.7 μM for epitifibate,[31] and 0.04 mM for aspirin[32]). This agreement is impressive given that the literature assays are fundamentally different and were inferred from platelet shape change or aggregation measurements. Table S5 summarizes the different methods used to determine literature IC_{50} values for these inhibitors. It is important to note that the plate reader readout is orders of magnitudes more rapid compared to the microscopy-based measurement, as the latter requires the acquisition of hundreds of images that then further require masking and image analysis to determine the signal intensity from each cell. Second, microscopy data is markedly more heterogenous both when comparing between cells in the same well and when comparing cells in different wells (Figure 4 and Figure S16). Of course, the plate reader instrument is significantly less sensitive as a detector, but it has the inherent advantage of averaging the intensity from millions of cells in each well, thus averaging the heterogeneity in signal caused by fluctuation in probe surface density and cell state. Although the sample preparation and cell incubation required ≈3 h to complete, the mechano-HCR plate reader readout for 6 different drug concentrations required less than 1 min. Therefore, this type of amplification and readout strategy represents an important milestone in enhancing the speed of data acquisition for characterizing cell traction forces.

Conclusion

In summary, we demonstrated that HCR can be triggered using a molecular biophysical event that exposes a cryptic initiator. While the HCR assay is widely used in mRNA detection in cells and tissue,[33] our work here represents the first example of using this amplification strategy for the quantification of specific pN events mediated by cell surface receptors. We applied the mechano-HCR assay to investigate the integrin receptor forces in fibroblasts and platelets, and showed that this readout offers approximately one order of magnitude enhancement in S/N when compared to direct quantification of duplex rupture. As a result of this enhanced signal, we showed the ability for direct readout of integrin tension using a conventional plate reader without having to employ high-magnification EMCCD-equipped fluorescence microscopy. Importantly, this capability enabled screening of the traction forces generated by different cells and their response to drug treatment on a plate reader instrument in a rapid manner. The mechano-HCR signal is linearly proportional to the density of cells at lower cell densities, and this signal plateaus as cells reach confluency. We also determined the mechano-IC_{50}, defined here as the concentration of drug that diminishes integrin traction forces by 50%, for two representative cell models—NIH/3T3 fibroblasts, mouse platelets—and tested responses of different classes of drugs such as ROCK inhibitor, eptifibatide, and aspirin. The measured IC_{50} of each inhibitor closely agreed with reported values obtained using indirect methods that measure secondary signals and cell morphology. Currently, the gold standard for measuring platelet function employs aggregation assays which are highly sensitive and are used in the clinic.[34] The mechano-HCR assay offers a complementary and potentially more direct method of screening cell function by measuring receptor forces. This assay could also be useful in evaluating therapeutics for other diseases of altered cellular contractility, such as asthma and cardiomyopathies.[35] Moreover, the ability to conduct readout using a fluorescence plate reader may offer more convenient and accessible readout. Also note that because of the isothermal and enzyme-free conditions used for HCR, the mechano-HCR assay carries advantages in sample preparation and reagent storage when compared to enzyme-catalyzed amplification such as mechanically induced catalytic amplification reaction.[36] This feature allows potential integration of mechano-HCR with automated plate washers and plate imagers for higher throughput and automation. Note that mechano-HCR reflects the traction forces present at earlier time points because of the kinetics of HCR. Assays such as the "exchange-mechano-HCR assay", where the hairpin monomers are barcoded with different dyes and washed into the sample periodically, may offer the ability to time-stamp the mechano-HCR signals. Furthermore, advances in HCR, such as controlled HCR,[22] branched HCR,[37] and FRET HCR,[38] suggest future directions to improve mechano-HCR S/N, convenience by reducing wash steps, and other advantages in simplifying quantification to address the challenge. Finally, mechano-HCR offers important potential in the adoption for applications such as medium-throughput drug and cell screening in both biological research and clinics.

Acknowledgements

K.S. acknowledges support from NIH R01GM124472 and R01GM131099, and NSF DMR-1905947. Y.K. acknowledges support from NSF DMR-1654485.

Conflict of Interest

The authors declare no conflict of interest.

Keywords: biosensors · cellular receptor tension · drug screening · hybridization chain reaction · nanotechnology

[1] a) B. Ladoux, R.-M. Mège, *Nat. Rev. Mol. Cell Biol.* **2017**, *18*, 743–757; b) A. W. Orr, B. P. Helmke, B. R. Blackman, M. A.

Schwartz, *Dev. Cell* **2006**, *10*, 11 – 20; c) Y. Liu, L. Blanchfield, V. P.-Y. Ma, R. Andargachew, K. Galior, Z. Liu, B. Evavold, K. Salaita, *Proc. Natl. Acad. Sci. USA* **2016**, *113*, 5610 – 5615; d) K. H. Vining, D. J. Mooney, *Nat. Rev. Mol. Cell Biol.* **2017**, *18*, 728 – 742.
[2] J. M. Brockman, K. Salaita, *Front. Phys.* **2019**, *7*, 14.
[3] a) L. H. Ting, S. Feghhi, N. Taparia, A. O. Smith, A. Karchin, E. Lim, A. S. John, X. Wang, T. Rue, N. J. White, *Nat. Commun.* **2019**, *10*, 1204; b) D. R. Myers, Y. Qiu, M. E. Fay, M. Tennenbaum, D. Chester, J. Cuadrado, Y. Sakurai, J. Baek, R. Tran, J. C. Ciciliano, *Nat. Mater.* **2017**, *16*, 230 – 235; c) M. E. Carr, *Cell Biochem. Biophys.* **2003**, *38*, 55 – 78.
[4] Y. Liu, K. Galior, V. P.-Y. Ma, K. Salaita, *Acc. Chem. Res.* **2017**, *50*, 2915 – 2924.
[5] a) D. R. Stabley, C. Jurchenko, S. S. Marshall, K. S. Salaita, *Nat. Methods* **2012**, *9*, 64 – 67; b) V. P. Y. Ma, K. Salaita, *Small* **2019**, *15*, 1900961.
[6] Y. Zhang, C. Ge, C. Zhu, K. Salaita, *Nat. Commun.* **2014**, *5*, 5167.
[7] S. B. Kim, R. Nishihara, D. Citterio, K. Suzuki, *Bioconjugate Chem.* **2016**, *27*, 354 – 362.
[8] R. Ma, A. V. Kellner, V. P.-Y. Ma, H. Su, B. R. Deal, J. M. Brockman, K. Salaita, *Proc. Natl. Acad. Sci. USA* **2019**, *116*, 16949 – 16954.
[9] Z. Wan, X. Chen, H. Chen, Q. Ji, Y. Chen, J. Wang, Y. Cao, F. Wang, J. Lou, Z. Tang, *eLife* **2015**, *4*, e06925.
[10] a) Y. Zhang, Y. Qiu, A. T. Blanchard, Y. Chang, J. M. Brockman, V. P.-Y. Ma, W. A. Lam, K. Salaita, *Proc. Natl. Acad. Sci. USA* **2018**, *115*, 325 – 330; b) K. M. Spillane, P. Tolar, *J. Cell Biol.* **2017**, *216*, 217 – 230.
[11] X. Wang, T. Ha, *Science* **2013**, *340*, 991 – 994.
[12] M. H. Jo, W. T. Cottle, T. Ha, *ACS Biomater. Sci. Eng.* **2019**, *5*, 3856 – 3863.
[13] C. Gaudet, W. A. Marganski, S. Kim, C. T. Brown, V. Gunderia, M. Dembo, J. Y. Wong, *Biophys. J.* **2003**, *85*, 3329 – 3335.
[14] J. Adams, *J. Histochem. Cytochem.* **1992**, *40*, 1457 – 1463.
[15] a) J. S. Gootenberg, O. O. Abudayyeh, M. J. Kellner, J. Joung, J. J. Collins, F. Zhang, *Science* **2018**, *360*, 439 – 444; b) X. Ding, K. Yin, Z. Li, R. V. Lalla, E. Ballesteros, M. M. Sfeir, C. Liu, *Nat. Commun.* **2020**, *11*, 4711.
[16] R. M. Dirks, N. A. Pierce, *Proc. Natl. Acad. Sci. USA* **2004**, *101*, 15275 – 15278.
[17] H. M. Choi, V. A. Beck, N. A. Pierce, *ACS Nano* **2014**, *8*, 4284 – 4294.
[18] W. J. Galush, J. A. Nye, J. T. Groves, *Biophys. J.* **2008**, *95*, 2512 – 2519.
[19] a) R. Glazier, J. M. Brockman, E. Bartle, A. L. Mattheyses, O. Destaing, K. Salaita, *Nat. Commun.* **2019**, *10*, 4507; b) J. M. Brockman, H. Su, A. T. Blanchard, Y. Duan, T. Meyer, M. E. Quach, R. Glazier, A. Bazrafshan, R. L. Bender, A. V. Kellner, *Nat. Methods* **2020**, *17*, 1018 – 1024.
[20] a) M. Mosayebi, A. A. Louis, J. P. Doye, T. E. Ouldridge, *ACS Nano* **2015**, *9*, 11993 – 12003; b) K. Hatch, C. Danilowicz, V. Coljee, M. Prentiss, *Phys. Rev. E* **2008**, *78*, 011920.
[21] M. Pfaff, K. Tangemann, B. Müller, M. Gurrath, G. Müller, H. Kessler, R. Timpl, J. Engel, *J. Biol. Chem.* **1994**, *269*, 20233 – 20238.
[22] C. A. Figg, P. H. Winegar, O. G. Hayes, C. A. Mirkin, *J. Am. Chem. Soc.* **2020**, *142*, 8596 – 8601.
[23] N. Gustafsson, S. Culley, G. Ashdown, D. M. Owen, P. M. Pereira, R. Henriques, *Nat. Commun.* **2016**, *7*, 12471.
[24] R. Krishnan, J.-A. Park, C. Y. Seow, P. V. Lee, A. G. Stewart, *Trends Pharmacol. Sci.* **2016**, *37*, 87 – 100.
[25] T. Ishizaki, M. Uehata, I. Tamechika, J. Keel, K. Nonomura, M. Maekawa, S. Narumiya, *Mol. Pharmacol.* **2000**, *57*, 976 – 983.
[26] E. Sahai, T. Ishizaki, S. Narumiya, R. Treisman, *Curr. Biol.* **1999**, *9*, 136 – 145.
[27] a) J. M. Gibbins, *J. Cell Sci.* **2004**, *117*, 3415 – 3425; b) B. Estevez, X. Du, *Physiology* **2017**, *32*, 162 – 177.
[28] P. T. Investigators, *N. Engl. J. Med.* **1998**, *339*, 436 – 443.
[29] a) J. Vane, R. Botting, *Thromb. Res.* **2003**, *110*, 255 – 258; b) G. Roth, P. W. Majerus, *J. Clin. Invest.* **1975**, *56*, 624 – 632.
[30] a) B. Z. Paul, J. L. Daniel, S. P. Kunapuli, *J. Biol. Chem.* **1999**, *274*, 28293 – 28300; b) M. Uehata, T. Ishizaki, H. Satoh, T. Ono, T. Kawahara, T. Morishita, H. Tamakawa, K. Yamagami, J. Inui, M. Maekawa, *Nature* **1997**, *389*, 990 – 994.
[31] X. Wang, R. T. Dorsam, A. Lauver, H. Wang, F. A. Barbera, S. Gibbs, D. Varon, N. Savion, S. M. Friedman, G. Z. Feuerstein, *J. Pharmacol. Exp. Ther.* **2002**, *303*, 1114 – 1120.
[32] M. Abe, Y. Ozawa, *Biosci. Biotechnol. Biochem.* **2006**, *70*, 2494 – 2500.
[33] H. M. Choi, M. Schwarzkopf, M. E. Fornace, A. Acharya, G. Artavanis, J. Stegmaier, A. Cunha, N. A. Pierce, *Development* **2018**, *145*, dev165753.
[34] R. Paniccia, R. Priora, A. A. Liotta, R. Abbate, *Vasc. Health Risk Manage.* **2015**, *11*, 133.
[35] a) K. Galior, V. P. Y. Ma, Y. Liu, H. Su, N. Baker, R. A. Panettieri, Jr., C. Wongtrakool, K. Salaita, *Adv. Healthcare Mater.* **2018**, *7*, 1800069; b) P. G. Vikhorev, N. N. Vikhoreva, *Int. J. Mol. Sci.* **2018**, *19*, 2234.
[36] V. P. Y. Ma, Y. Liu, K. Yehl, K. Galior, Y. Zhang, K. Salaita, *Angew. Chem. Int. Ed.* **2016**, *55*, 5488 – 5492; *Angew. Chem.* **2016**, *128*, 5578 – 5582.
[37] S. Bi, M. Chen, X. Jia, Y. Dong, Z. Wang, *Angew. Chem. Int. Ed.* **2015**, *54*, 8144 – 8148; *Angew. Chem.* **2015**, *127*, 8262 – 8266.
[38] J. Guo, C. Mingoes, X. Qiu, N. Hildebrandt, *Anal. Chem.* **2019**, *91*, 3101 – 3109.

Manuscript received: June 8, 2021
Accepted manuscript online: July 9, 2021
Version of record online: July 29, 2021

